Automotive Science and Engineering

Journal Homepage: ase.iust.ac.ir

Analytical Model for Estimating the Motion of the Liquid Metal Droplet in Electromagnetic Micropump

Mohsen Karmozdi [1*]

[1]Department of Mechanical Engineering, K. N. T. University of Technology, Tehran, 1999143344, Iran

ARTICLE INFO	ABSTRACT
	The liquid metal droplets in the mercury magnetic reciprocating micropump are actuated by Lorentz force and reciprocated inside some sub-channels. The droplets in sub-channel act as pistons to pump the working fluid. The initial step in establishing the performance of the mercury magnetic reciprocating micropumps is to study the motion of droplet inside the channel. The extraction of the analytic equation governing the droplet motion inside the channel is complicated due presence of electromagnetic fields and three dimensional effects of the flow. Further, the existence of a pumped fluid in contact with the droplet and the adhesion force due to small dimensions are considered as the other reasons. In this study, the forces operating on the droplet were figured out by the Lagrangian approach and lumped mass assumption for the droplet. Accordingly, forces less than 5% of the actuation force were eliminated from the motion equation of droplet employing dimensional analysis. The simplified equation was presented as an ordinary differential equation and solved numerically. In addition to the analytic solution, the issue was experimentally investigated for a case study. The analytic and empirical results accord well with one another. The method pointed out in this study can be applied to predict the droplet motion in various microsystems.

1. Introduction

In recent years, terms like "integrated analyst microsystems" and "lab-on-a-chip" have become well-established concepts in the field of research. These systems are designed to facilitate the analysis of sample displacement, reactions, separation, and identification within compact, chip-sized devices. A key component of any microfluidic system is the micropump, which is responsible for moving fluid. Micropumps are classified according to their actuation methods, including electro-osmotic, electrostatic, thermal, pneumatic, thermo-pneumatic, piezoelectric, and magnetohydrodynamic (MHD) types. Moghadam et al. [1] investigated a rotary positive displacement micropump that utilized Lorentz force to drive a liquid metal droplet (LMD) through a circular channel. The moving LMD acted as a piston, pumping air through the channel. Karmozdi (2013) [2] extended this concept by proposing the Magneto Mercury Reciprocating (MMR) micropump, which combined the benefits of both reciprocating and MHD micropumps. In this design, LMDs functioned as pistons within separate sub-channels to pump air through the microchannel. The MMR

micropump demonstrated several advantages, such as high performance, the absence of moving mechanical parts, cost-effective and simple manufacturing, valve-free operation, and independence from high voltage or temperature control. It was also unaffected by pH, ambient temperature, or surface charges, produced no heat, and worked effectively at higher flow rates. However, despite these promising characteristics, further research on optimizing its parameters was necessary. Subsequent researches by Haghayegh and Kazemi [3, 4] experimentally analyzed the effects of outlet aperture shape and actuation frequency on LMD motion within the MMR micropump. Their findings revealed that the maximum droplet displacement occurred at an actuation frequency of 10 Hz and an 80-degree angle between the LMD sub-channel aperture and the main channel. The use of LMDs as pistons in microsystems is an innovative approach, which requires further investigation to optimize performance. Understanding LMD motion is critical, not only for enhancing the MMR micropump but also for broader applications where droplet motion plays a key role.

For example, Lee and Chang [5] developed a microsystem in which surface tension served as the actuation force. In their system, an LMD inside a capillary tube containing an electrolyte was driven by localized surface tension modification through an applied electric potential. Similarly, Shabani and Cho [6] introduced a micropump that employed electro-wetting on a dielectric surface to generate pressure gradients within a droplet, enabling fluid pumping. Electro-wetting has gained significant attention in recent years, with applications in various fluidic and electro-optic devices. Pooyan and Passandideh [7] studied mercury droplet motion within rectangular microchannels driven by electro-wetting actuation and explored the impact of channel geometry. Their results showed that increasing the channel height or width enhanced the droplet velocity for a constant droplet volume. They also observed an inverse proportionality between droplet length and velocity. Palma and Deegan [8] demonstrated droplet actuation via photoelectrowetting, eliminating the need for electrode arrays. They measured the droplet speed's dependence on applied potential, laser intensity, fluid viscosity, and droplet size, achieving a maximum velocity of 13 mm/s.

Droplet-based actuation offers several advantages, such as reduced motion resistance and the absence of direct contact between solid components. However, challenges such as droplet collapse, deviation from the intended motion path, and difficulty in controlling droplet movement limit its applicability compared to solid-part actuation. To effectively control droplet motion in a channel, a thorough understanding of the governing mechanics is essential.

In practice, the governing equations for LMD motion in the MMR micropump are complex due to the unsteady, two-phase nature of the system. The interaction between the liquid metal (LM) and the surrounding continuous fluid (CF) requires solving the coupled Navier-Stokes and Maxwell equations in three dimensions, making an analytical solution highly challenging.

This study aims to derive a simplified analytical equation governing LMD motion within the MMR micropump. The complexity of the force equations arising from the interplay of electrical and magnetic fields within a fluid-filled channel makes an exact analytical solution infeasible. To address this, two key simplifications were made: (1) adopting a Lagrangian approach, wherein the observer follows the moving LMD, and (2) treating the droplet as a lumped mass, neglecting internal motions due to its small size. Additionally, forces with negligible magnitudes were omitted after order-of-magnitude analysis. The resulting simplified equation allowed for plotting LMD motion curves, which were subsequently validated through experimental results.

2. Theory

As shown in Figure 1, two electrodes positioned at the sides of the sub-channel carry electrical current to the liquid metal droplet (LMD). According to the Lorentz force principle, when an electrical current flows through the LMD in the y-direction within a magnetic field oriented in the z-direction, a Lorentz force (F_L) is exerted on the LMD, propelling it in the x-direction. Reversing the current direction in the electrodes inverts the Lorentz force, causing the LMD to move backward. Consequently, this force serves as an actuation mechanism to pump a working fluid, such as air. By placing multiple sub-channels containing LMD adjacent to a main microchannel and actuating them, working fluid pumping is achieved. The magnitude of the actuation Lorentz force (F_L) is given by:

$$F_L = I \, B \, w \tag{1}$$

where w represents the channel width, I denotes the electric current, and B is the magnetic field [2]. The actuation Lorentz force must provide sufficient inertia to overcome the resistance forces acting against the droplet's motion. The primary resistance forces acting on the LMD include wall friction (F_S), the dynamic contact angle hysteresis force (F_H) at the droplet-continuous fluid (CF) interface with the wall, and the CF forces at the droplet-CF contact surface (Figure 1). If the channel is laid horizontally, the buoyancy and gravitational forces are perpendicular to the channel direction and do not contribute to the droplet's motion equation along the x-axis. The forces acting on the LMD are introduced as follows:
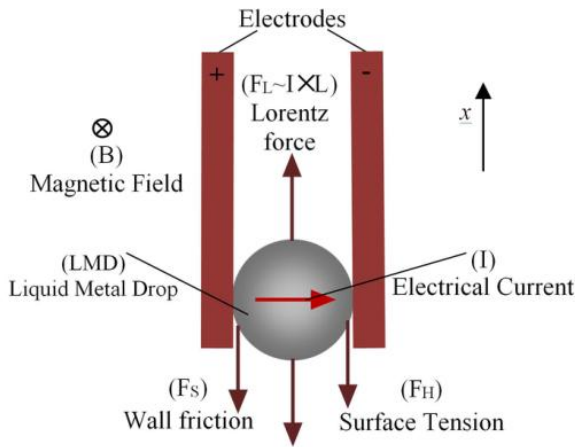

Figure 1. The Schematic of LMD actuation in magnetohydrodynamic micropumps (MMR).

Dynamic contact angle hysteresis force

A moving droplet on a hydrophobic surface exhibits different advancing and receding dynamic contact angles, resulting in a resistance force known as contact angle hysteresis (F_H), defined as [9]:

$$F_H = 2 R \eta \gamma J \tag{2}$$

where η represents the contact line ratio, γ denotes the liquid-vapor surface tension, and R shows the droplet radius. The contact angle hysteresis, J, is given by

$$J = cos(\theta_a) - cos(\theta_r) \tag{3}$$

where θ_a is the advancing dynamic contact angle and θ_r is the receding dynamic contact angle. The dynamic contact angle depends on droplet velocity. Hoffman formulated an empirical relationship for dynamic contact angle hysteresis, which was later simplified by Tanner as:

4757 Automotive Science and Engineering (ASE)

$$\theta_d^3 - \theta_s^3 = A\, Ca_d \tag{4}$$

where θ_d is the dynamic contact angle, θ_s is the static contact angle, and A is the Hoffman coefficient, with a value of 94 [10]. The capillary number, Ca_d, is given by:

$$Ca_d = \mu_d\, u_d/\gamma \tag{5}$$

where μ_d is the absolute viscosity of the droplet and u_d is its velocity. The sign of the velocity in this equation must be correctly accounted for: positive in the advancing meniscus and negative in the receding meniscus.

Wall friction force

The wall friction force (F_s) results from shear stress at the liquid boundary and is given by:

$$F_s = 1/2\, f\, \rho_d u_d^2\, S_w \tag{6}$$

where S_w is the wetted wall surface area, ρ_d is the LMD density, and f is the Fanning friction coefficient. Because the motion is accelerated, the boundary layer is not fully developed, requiring consideration of its effects. According to Blasius' solution [11], the wall friction coefficient is:

$$f = 0.664/\sqrt{Re_x} \tag{7}$$

where Re_x is the Reynolds number based on droplet position in the channel:

$$Re_x = u_d\, x/\nu_d \tag{8}$$

where ν_d is the kinematic viscosity of the droplet and x is its position from the start of motion. The geometric parameters are illustrated in Figure 1.

CF forces

Forces exerted by the CF on the LMD include Basset skin, added mass, and drag [12]. A lift force perpendicular to the droplet's motion ((in the y-direction) also exists but is not considered in the x-direction motion equation.

Drag force

The maximum drag coefficient is estimated, as inaccuracies in its calculation are negligible due to its

Mohsen Karmozdi

small magnitude compared to dominant forces. The drag force (F_D) is:

$$F_D = 1/2 \, C_D \, \rho_c \, S \, (u_d - u_c)^2 \qquad (9)$$

where ρ_c is the CF density, S is the droplet surface area in the motion direction, u_c is the CF velocity, and C_D is the drag coefficient and is estimated as:

$$C_D = C_1 C_2 C_3 \, (24/Re_c) \qquad (10)$$

where correction factors C_1, C_2, and C_3 account for inertia, internal droplet motion, and wall effects, respectively. The Reynolds number of the CF, Re_c is given by:

$$Re_c = D_d(u_d - u_c)/\nu_c \qquad (11)$$

where D_d is the hydraulic diameter of the droplet and ν_c is the CF kinematic viscosity. Schiller and Naumann [13] proposed ($1 < Re_c < 1000$):

$$C_1 = (1 + 0.15 \, Re_c^{0.687}) \qquad (12)$$

In addition, the correction factor of internal motion of droplet is always less than one [14].

Considering maximal drag, $C_2 = 1$ and $C_3 = 12$ (based on Faxen's modification [15]), leading to:

$$C_D = 288 \, (1 + 0.15 \, Re_c^{0.687})/Re_c \qquad (13)$$

For $Re_c > 1$, $C_D < 332$.

Added mass and Basset forces

The reaction of the CF to the motion of the LMD moving inside it brought about a change in the inertia of the LMD. Increase or decrease in the acceleration of the LMD in the CF required an increase or decrease in the acceleration of an amount of CF around the LMD. This amount of CF is called the added mass. The Basset force, as the history force, was created due to delay in the development of the CF boundary layer on the LMD by a change in the relative velocity. This force is often neglected because significantly complicates the equations of motion. But, Daitche [16] showed that the Basset force can have a considerable effect in turbulence. The analytical solution for the both aforementioned forces is only feasible at low Reynolds numbers. The development of these equations for the LMD with high Reynolds is only possible through introduction of experimental coefficients similar to the drag coefficients for all the forces. Odar and Hamilton [17] empirically studied the motion of a sphere in a simple

harmonic motion, and accordingly, added mass (F_A) and Basset (F_B) forces are defined as follows [18]:

The CF's reaction to LMD motion alters its inertia. Added mass (F_A) and Basset (F_B) forces are expressed as [18]:

$$F_A = 1/2\rho_c V(Du_c/Dt - du_d/dt) \qquad (14)$$

$$F_B = 6R^2\sqrt{\pi\rho_c\mu_c} \int_0^t \frac{d(u_c - u_d)}{dt'} \frac{dt'}{\sqrt{t - t'}} \qquad (15)$$

where V is the LMD volume and t is time. Basset force is often neglected due to complexity but may be significant in turbulent conditions [16].

According to (14) and (15) it is observed that to calculate the Basset force it is necessary to integrate the velocity gradient of fluid and solid body during the time. In what follows, the orders of magnitude of these two forces in comparison with other forces acting on LMD were identified by using scaling analysis. As long as this force had a negligible effect on the acceleration of the droplet and it could be overlooked, the complexities associated with integrating the velocity gradient with respect to time were obviated.

Scaling analysis of forces (order of magnitude)

Taking all the forces on the droplet into account complicates the governing equation. In this section, the order of magnitude of above mentioned forces were identified and the low-order forces were neglected. For this, the actuation Lorentz force was used as a reference and all retention forces were compared to that to find the order of magnitude of each force.

Initially, characteristic parameters were defined for nondimensionalization. The distance between the two electrodes, which is equal to the channel width (w) and LMD diameter, was employed as the characteristic length. A characteristic time was assumed to be equal to $\tau = \sqrt{\rho_d w^3/IB}$ and characteristic velocity (U) was defined as follows:

$$U = w/\tau = \sqrt{IB/\rho_d w} \qquad (16)$$

Next, four nondimensional constants were defined to simplify the equations as mentioned.

Table 1. Non-dimensional constants of the issue

parameter	Sym.	Equation	value for the case study
density ratio	$\bar{\rho}$	ρ_d/ρ_c	1.17 E+4
viscosity ratio	$\bar{\mu}$	μ_d/μ_c	81.5
constant Reynolds number	Re_0	wU/ν_d	542
constant capillary number	Ca_0	$\mu_d U/\gamma$	9.50 E-5

Table 1 shows nondimensional constants, where μ_d represents the LMD viscosity and μ_c denotes the viscosity of CF. It should be considered that the constant Reynolds and capillary numbers were only two nondimensional parameters used to simplify the equations. They should not be confused with the Reynolds and capillary numbers of flow (Re_x and Ca_d) calculated from Eq.s (5) and (8) which determine regime of the flow. Finally, all forces acting on the LMD were compared with the actuation Lorentz force. The ratio of retention forces to the Lorentz force are shown in Table 2.

Table 2. Forces ratio to Lorentz force

Force	Ratio to Lorentz force (F/FL)	Order of magnitude
Drag, F_D	$\left(\frac{1}{2}\frac{S}{w^2}\right)C_D\frac{1}{\bar{\rho}}u^{*2}$	5 %
Added mass, F_A	$\left(\frac{1}{2}\frac{V}{w^3}\right)\frac{1}{\bar{\rho}}\frac{du^*}{dt^*}$	0.01 %
Basset, F_B	$\frac{3\sqrt{\pi}}{2}\frac{1}{\sqrt{\bar{\rho}\bar{\mu}Re_0}}\int_0^{t^*}\frac{du^*}{dt'}\frac{dt'}{\sqrt{t^*-}}$	1%
Wall friction, F_S	$\left(0.332\frac{S_w}{w^2}\right)\frac{1}{\sqrt{Re_0}}\sqrt{\frac{u^{*3}}{x^*}}$	-
Contact angle hysteresis , F_H	$\eta\frac{1}{Re_0 Ca_0}J(u^*)$	-

Values in the Table 2 were calculated based on the following assumptions:

$$\bar{\rho} > 10000, \bar{\mu} > 1, Re_0 > 1$$
$$u^* < 2, du^*/dt^* < 5, Re_c > 1 \tag{17}$$

It is shown further that the above assumptions were valid for the LMD motion in MMR micropump. According to Table 2, the drag, added mass, and Basset forces had an order of magnitude less than 5% of the actuation Lorentz force; therefore, their effects were neglected. As a result, by eliminating these low-order forces, the equation of motion for LMD was rewritten as the following equation:

$$\rho_d V du_d/dt = wIB - \eta w \gamma J(u^*) - 1/2\, S_w f \rho_d u_d^2 \tag{18}$$

To nondimensionalize the equation, the nondimensional parameters of the LMD were defined as nondimensional time $t^* = t/\tau$, nondimensional position $x^* = x/w$, nondimensional velocity $u^* = u/U$, and nondimensional acceleration $a^* = du^*/dt^*$. By substituting the nondimensional parameters into the problem, the nondimensional equation of motion for the LMD was equal to:

$$\frac{V}{w^3} a^* = 1 - \frac{\eta}{Re_0 Ca_0} J(u^*) - \frac{1}{2}\frac{S_w}{w^2}f(u^*)u^{*2} \tag{19}$$

where $\theta_{s,a}$ and $\theta_{s,r}$ represent the advancing and receding static contact angles, respectively. According to Eq. (4), the contact angle hysteresis was calculated from the following equation:

$$J(u^*) = cos\left(\sqrt[3]{\theta_{s,a}^3 + A\, Ca_0\, u^*}\right) - cos\left(\sqrt[3]{\theta_{s,r}^3 - A\, Ca_0\, u^*}\right) \tag{20}$$

The wall friction coefficient was calculated through (7). The relation between the instantaneous Reynolds (Re_x) and constant Reynolds (Re_0) was according to the following equation:

$$Re_x = Re_0\, x^*\, u^* \tag{21}$$

Therefore, Eq. (7) was written as $f(u^*) = 0.664/\sqrt{Re_0\, x^*\, u^*}$. Finally, the nondimensional governing equation of motion of LMD is equal to:

$$\frac{V}{w^3}a^* = 1 - \frac{\eta}{Re_0\, Ca_0}\left[cos\left(\sqrt[3]{\theta_{s,a}^3 + A\, Ca_0\, u^*}\right) - cos\left(\sqrt[3]{\theta_{s,r}^3 - A\, Ca_0\, u^*}\right)\right] - \frac{S_w}{w^2}\frac{0.332}{\sqrt{Re_0}}\sqrt{\frac{u^{*3}}{x^*}} \tag{22}$$

The above equation predicts the motion of not only the LMD in MMR micropump, but also any droplet moving in a square cross-section channel containing continuous fluid. The following assumptions are made in the derivation of Eq. (22):

The LMD flow in the channel is laminar and the CF flow around LMD is transient. The LMD velocity and consequently, the Reynolds numbers (Re_c and Re_x) were extracted by solving Eq. (22), and accordingly, the validity of this condition was confirmed.

Conditions (17) are valid and consequently, CF forces (drag, added mass and Basset) are insignificant in comparison to other forces. Conditions (17) were

validated by calculation of constant values of the issue. Moreover, by calculating all forces, it was shown that CF forces were negligible in comparison to the actuation Lorentz force.

Besides all of these, the issue was empirically investigated for a case study and the validity of the analytical model was confirmed by the imperial results.

Table 3. The materials properties at 300K, 1 bar [19]

| Sym.	Quantity	Dim.	Value
ρ_d	Density of mercury	kg/m3	13529
μ_d	Absolute viscosity of mercury	mPa s	1.517
ν_d	Kinematic viscosity of mercury	mm2/s	0.1121
ρ_c	Density of air	kg/m3	1.161
μ_c	Absolute viscosity of air	(μPa s	18.6
ν_c	Kinematic viscosity of air	mm2/s	16.0
γ	Mercury surface tension	N/m	0.485
$\theta_{a,s}$	Mercury Advancing static contact angle	°	138 [20]
$\theta_{r,s}$	Mercury Receding static contact angle	°	128 [20]
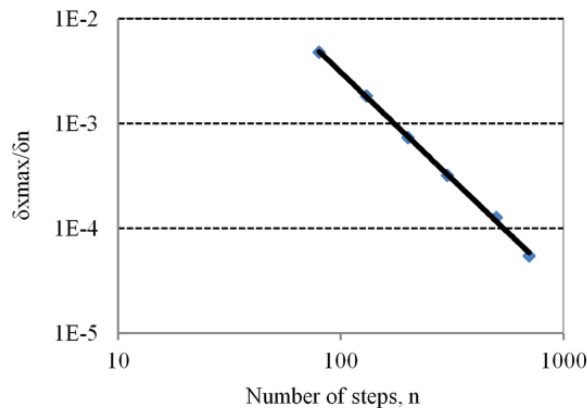
Figure 2. The variations of total length passed by LMD along the channel vs. the number of time steps.

Case study

LMD and CF in the MMR micropump were mercury and air, respectively, and the properties of fluids are given in Table 3. In the issue, actuation force was equal to $F_L = 0.05 mN$, and the channel width was $w = 2mm$. Accordingly, the characteristic

time and velocity were equal to $\tau = 65.8 ms$ and $U = 0.03 m/s$. The calculated constant values are presented in Table 1 and conditions (17) are confirmed.

Eq. (22) was discretized and solved implicitly with initial conditions of $u^*(0) = 0$ and $x^*(0) = 0$. The results were obtained until $t^* = 1$ ($t = \tau$). The dependence of results to time step (n) was checked by solving the equation for different time steps. The total length passed by LMD along the channel was calculated (x_{max}). The variations of results with change in the number of time steps ($\delta x_{max}/\delta n$) is presented in Figure 2. According to the results, the time step of 700 was selected by an error of less than 10-4. Figure 3(a) illustrates the nondimensional acceleration of LMD vs. time. Next, the velocity and position were derived by integrating the acceleration with respect to time and are presented in Figure 3(b, c). It is observed that the acceleration was positive and the LMD motion was increasing in velocity. According to Eq. (1), the actuation Lorentz force was independent of the LMD velocity, whereas the resistance forces increased by increasing the velocity. Therefore, as shown in Figure 3(a), although the velocity vs. time was a strictly increasing function, the acceleration curve was strictly decreasing function of time.

Figure 4(a) displays the ratio of the drag, added mass, and Basset forces to the actuation force. In the calculation of these forces, the maximum relative velocity of the LMD and CF was assumed ($u_d - u_c = u_d$) and as a result, the maximum of CF forces was obtained. As illustrated, all of CF forces were below the threshold level of 1% and therefore the assumption of neglecting these forces was valid.

Figure 4(b) indicates the ratio of the wall friction, dynamic contact angle hysteresis, and the sum of the CF forces to the actuation Lorentz force. According to Eq.s (2) and (6), the dynamic contact angle hysteresis (F_H) and the wall friction force (F_S) both increased by increasing the velocity of the droplet. As shown in Figure 4(b), in the first part of the motion, the dominant retention force was the dynamic contact angle hysteresis, and the wall friction was negligible, but the wall friction increased more rapidly by increasing the velocity of LMD.
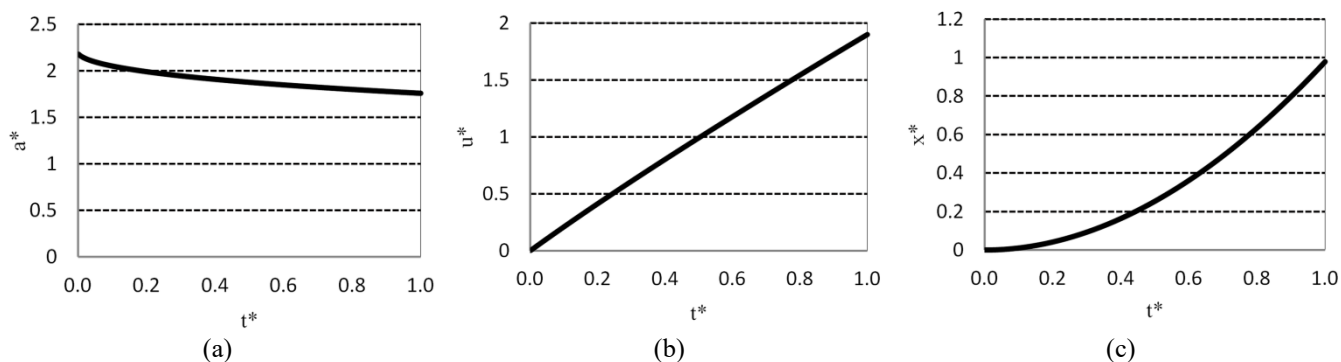
(a)

(b)

(c)

Figure 3. The analytical results of LMD motion vs. non-dimensional time for the issue (a) The non-dimensional acceleration, (b) The non-dimensional velocity, (c) The non-dimensional position
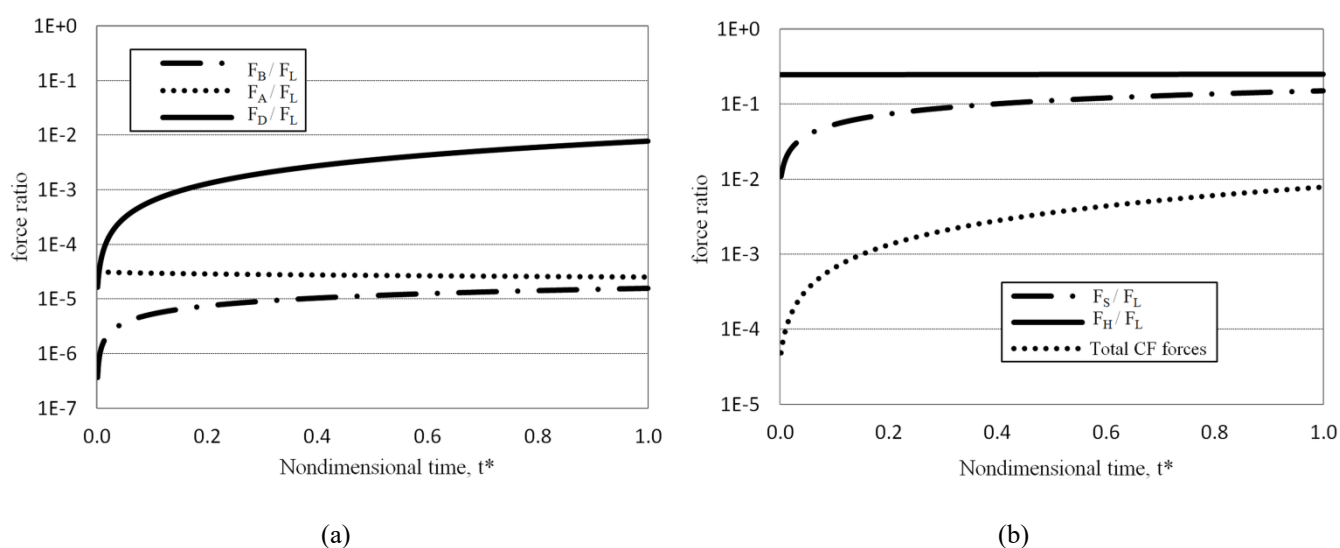

(a)

(b)

Figure 4. The percent of the retention forces acting on LMD respect to Lorentz force (FL) vs. non-dimensional time: (a) all acting forces, (b) CF forces.
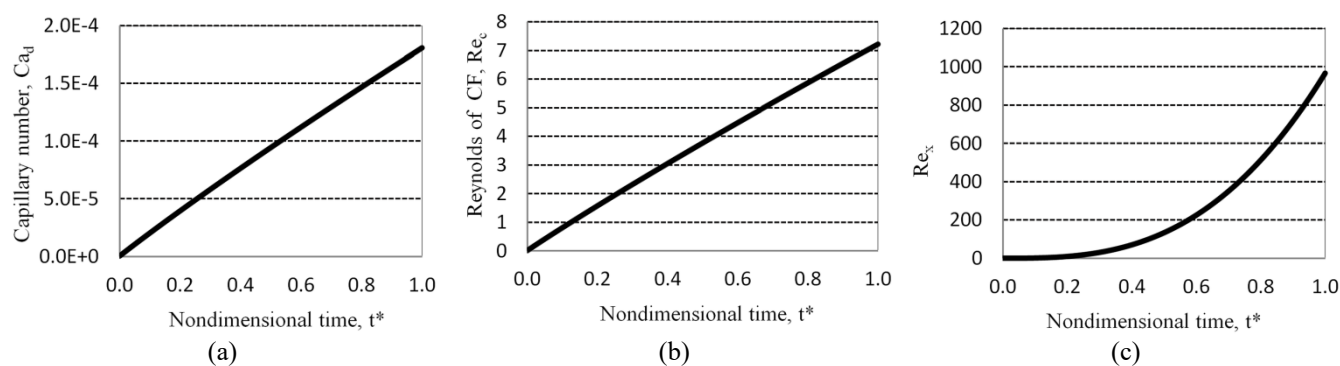

(a)

(b)

(c)

Figure 5. The Instantaneous nondimensional numbers vs. nondimensional time (a) capillary number for LMD, (b) Reynolds for CF (air), (c) Reynolds for LMD.

4761   Automotive Science and Engineering (ASE)

The capillary number vs. time is presented in Figure 5(a). It is observed that the capillary number for this flow is very small ($Ca_d < 10^{-3}$). Figure 5(b) and (c) illustrate the Reynolds of the LMD and CF during the motion period. As shown, the aforementioned assumptions of laminar flow for LMD and transient flow for boundary layer of CF around LMD were valid.

3. Experimental Validation

The case study was experimentally examined in the lab to validate the analytical model. As illustrated in Figure 1, the LMD was actuated in the channel by the Lorentz force. The required channel was carved on Plexiglass using the CNC machine model DAHLIH-37508-00017. To connect the body parts of the channel, Chloroform, a solvent for Plexiglass, was applied to the contact surfaces, which were then pressed together for 10 minutes. After assembling the body, the mercury droplet, serving as the LMD, was placed inside. Electrical current was applied to the LMD using two electrodes placed on the sides of the channel (Figure 1). The end of the channel was sealed with thermal adhesive after positioning the electrodes. A permanent neodymium magnet generated the required magnetic field, with the intensity in the channel measured at 50±1mT using an AC/DC Teslameter (model MG-3002). A LABVIEW computer program was used to generate the desired electrical signal, which was converted to electrical voltage using a data acquisition board (Advantech PCI1711L). The data were transferred to the PCI-8710 terminal. An electrical amplifier board with a maximum current of ±0.5A amplified the signals produced by LABVIEW. The output current of this amplifier board was applied to the LMD via the electrodes. An interface board was designed to generate a bi-directional electrical current. In the next stage, the desired current was created with a square wave, adjustable in both positive and negative directions. The amplifier board output was connected to the two electrodes inside the channel, resulting in an electrical current passing through the LMD. As the electrical current passed through the LMD in the presence of the magnetic field, the Lorentz force was applied in the channel direction, causing movement of the LMD.

To capture the motion and measure displacement, a Nikon J4 camera with a resolution of 416x144 pixels and a shooting speed of 1200 fps was used. The film obtained was analyzed using Droplet Morphometry and Velocimetry (DMV) software. By tracking the LMD position in each frame and considering the frame rate, data associated with the position and time of the LMD were extracted. The experimental test was conducted with the parameters shown in Table 3. The values of Re_0 and Ca_0 for this study, calculated by characteristic velocity, are provided in Table 1. The results of the analytical solutions and experiments, with error bars of 0.05, are illustrated in Figure 6. It was observed that the analytical curve provides the best fit to the experimental results, confirming the validity of the analytical model. Therefore, the analytical method presented is applicable and can be utilized to identify the motion of the LMD in MMR micropumps, as well as in any droplet system where the aforementioned assumptions are valid.
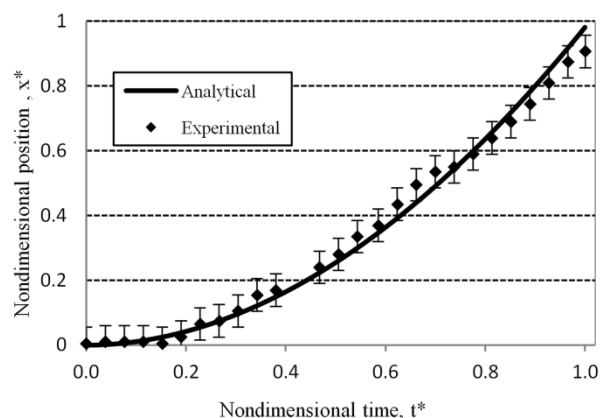

Figure 6. Analytical and experimental results comparison

4. Conclusion

The fundamental step in understanding the performance of microsystems, including MMR micropumps, is the investigation of droplet motion and the influence of various parameters on this motion. The LMD motion, actuated by the Lorentz force in a channel, was studied. The forces acting on the LMD were calculated using

the Lagrangian approach and the lumped mass assumption for the LMD. By nondimensionalizing the problem, the magnitude of the forces relative to the actuation Lorentz force was assessed. Several conditions were assumed to simplify the equations, and it was shown that the CF forces had a negligible effect, with an order of magnitude smaller than 5%. Consequently, the force equation for the LMD was derived by eliminating these insignificant CF forces. The governing equation, expressed as an ordinary differential equation (ODE), was applied to estimate the LMD motion in the MMR micropump and to enhance pump performance. The equation was solved through discretization, yielding results for acceleration, velocity, and position of the LMD over time.

Two steps were followed to validate the analytical model. First, it was demonstrated that all assumptions applied to the model were valid. Second, the CF forces were calculated and shown to contribute less than 1% of the Lorentz force. Additionally, the issue was experimentally investigated in the lab, validating the analytical model with empirical results. This study highlighted that, for identifying droplet motion in microsystems, the problem can be simplified using the Lagrangian approach and lumped mass assumption, along with dimensional analysis of forces. These methods allow for accurate results with acceptable precision.

References

[1]   M. E. Moghadam and M. B. Shafii, "Rotary magnetohydrodynamic micropump based on slug trapping valve," J. Microelectromech. Syst., vol. 20, pp. 260-269, 2011.

[2]   M. Karmozdi, A. Salari, and M. B. Shafii, "Experimental study of a novel Magneto Mercury Reciprocating (MMR) micropump, fabrication and operation," Sensors and Actuators A: Physical, vol. 194, pp. 277-284, 2013.

[3]   S. Haghayegh, S. Kazemi Abnavi, M. Karmozdi, M. B. Shafii, and A. Amini Nodoushan, "Experimental investigation on the effect of micro cavity - micro channel angle on the reciprocating motion of mercury in a micro cavity," presented at the Int. Conf. Thermal, Material and Mechanical Eng. (ICTMME'2012), Singapore, 2012.

[4]   S. Kazemi Abnavi, S. Haghayegh, M. Karmozdi, M. B. Shafii, and A. Salari, "Experimental investigation on the effect of stimulating frequency on the reciprocating motion of mercury in a micro cavity," presented at the Int. Conf. Thermal, Material and Mechanical Eng. (ICTMME'2012), Singapore, 2012.

[5]   H. J. Lee and K. Chang-Jin, "Surface-tension-driven microactuation based on continuous electrowetting," J. Microelectromech. Syst., vol. 9, pp. 171-180, 2000.

[6]   R. Shabani and H. J. Cho, "Active surface tension driven micropump using droplet/meniscus pressure gradient," Sensors and Actuators B: Chemical, vol. 180, pp. 114-121, 2013.

[7]   S. Pooyan and M. Passandideh-Fard, "Investigation of the Effect of Geometric Parameters on EWOD Actuation in Rectangular Microchannels," Journal of Fluids Engineering, vol. 140, pp. 091104-091104-9, 2018.

[8]   C. Palma and R. D. Deegan, "Droplet Translation Actuated by Photoelectrowetting," Langmuir, vol. 34, pp. 3177-3185, 2018/03/13 2018.

[9]   W. C. Nelson, P. Sen, and C.-J. C. Kim, "Dynamic contact angles and hysteresis under electrowetting-on-dielectric," Langmuir, vol. 27, pp. 10319-10326, 2011.

[10]   J. Berthier and P. Silberzan, Microfluidics for Biotechnology, Norwood: Artech House, 2010, pp. 39–40.

[11]   I. G. Currie, Fundamental Mechanics of Fluids, 3rd ed., New York: McGraw-Hill, 2002, p. 324.

[12]   A. Salari, M. Karmozdi, R. Maddahian, and B. Firoozabadi, "Analytical study of single particle tracking in both free and forced vortices," Scientia Iranica, vol. 20, pp. 351-358, 2013.

[13]   L. Schiller and A. Naumann, "Über die grundlegenden Berechnungen bei der Schwerkraftaufbereitung," Z. Ver. Dtsch. Ing 77, vol. no. 12, pp. 318-320, 1933

[14]   R. Clift, J. R. Grace, and M. E. Weber, Bubbles, Drops, and Particles, New York: Academic Press, 1978, p. 33.

[15]   H. Faxen, "Die Bewegung einer starren Kugel langs der Achse eines mit zahrer Flbsigkeit gefiillten Rohres " Ark. Mat. Astron. Fys, vol. 17, pp. 1-28, 1923.

[16]   A. Daitche, "On the role of the history force for inertial particles in turbulence," Journal of Fluid Mechanics, vol. 782, pp. 567-593, 2015.

[17]   F. Odar and W. S. Hamilton, "Forces on a sphere accelerating in a viscous fluid," Journal of Fluid Mechanics, vol. 18, pp. 302-314, 1962.

[18]   E. E. Michaelides and A. Roig, "A reinterpretation of the Odar and Hamilton data on the unsteady equation of motion of particles," AIChE J., vol. 57, pp. 2997-3002, 2011.

[19]   D. R. Lide, ed., CRC Handbook of Chemistry and Physics, http://www.hbcpnetbase.com: CRC Press, 2005.

[20]   A. Mehrabi, "Numerical simulation of magneto mercury reciprocating micrpump," M.S. thesis, Mech. Eng. Dept, Sharif Univ. Technol., Tehran, 2014.